TABLE III
COMPARISON OF MEASURED OSCILLATOR PERFORMANCE WITH COMPUTATIONS OF TREW *et al.*

	2nd Harmonic		3rd Harmonic	
	Measured	Computed	Measured	Computed
Tuning Range %	3.2	3.8	5.1	17.2
Efficiency Variation (dB)	±0.5	±1.0	±0.3	±0.6
Phase Shift of Harmonic	-	45°	100-150	100

range. Table III shows qualitative agreement with previously published computer predictions by Trew *et al.* [5]. The method also has potential use for circuit diagnosis since the harmonics can be readily separated.

Both methods utilize magnetic field changes which could be obtained from small magnetic field-coils. These coils can be built to provide moderately fast tuning rates, suggesting that several tens of megahertz per microsecond is a distinct possibility. The ferrimagnetic resonator method requires an additional fixed magnetic field as indicated in Figs. 7, 8, and 9.

ACKNOWLEDGMENT

We thank G. Winkler and P. Röschmann of Philips Research Laboratories Hamburg for supplying the ferrite spheres and our colleagues Dr. L. K. Brundle, Dr. R. Davies, M. Pierrepont, and P. L. Sugar for valuable discussions.

This work has been carried out with part support of the Procurement Executive, Ministry of Defence, UK, and sponsored by DCVD.

REFERENCES

[1] B. H. Newton, "MIC TRAPATT oscillator for efficient *S*-band operation," *Electron. Lett.*, vol. 11 no. 14, p. 299, 1975.
[2] C. D. Corbey, B. H. Newton, and J. G. Summers, "Frequency stable MIC *S*-band and *C*-band pulsed TRAPATT oscillators," in *Proc. 5th European Microwave Conf.*, (Hamburg, Germany), 1975, p. 237.
[3] B. Glance, "A magnetically tunable microstrip IMPATT oscillator," *IEEE Trans. Microwave Theory Tech.*, vol. MTT-21, June 1973, p. 425.
[4] S. G. Liu, "Magnetically tunable TRAPATT oscillator," in *Proc. 1974 IEEE Int. Solid State Circuits Conf.*, p. 98.
[5] R. Trew, G. Haddad, and N. Masnari, "Operation of *S*-band TRAPATT oscillators with tuning at multiple harmonic frequencies," *IEEE Trans. Microwave Theory Tech.*, vol. MTT-23, p. 1043, Dec. 1975.
[6] R. Trew, "Properties of *S*-band TRAPATT diode oscillators," Ph.D. dissertation, Dep. Elec. Eng., Univ. of Michigan, 1975.
[7] W. von Aulock, *Handbook of Microwave Ferrite Materials*. New York: Academic, 1965.
[8] G. Winkler, "Substituted polycrystalline YIG with very low ferrimagnetic resonance linewidth and optical transparency," *IEEE Trans. Magn.*, vol. MAG. 7, p. 773, Sept. 1971.

Slots in Dielectric Image Line as Mode Launchers and Circuit Elements

KLAUS SOLBACH, MEMBER, IEEE

Abstract—**Slots in the ground plane of dielectric image lines are investigated using a planar resonator model. An equivalent circuit representation of the slot discontinuity is derived and the launching efficiency of the slot as a mode launcher is discussed. Slots are also demonstrated to be useful in the realization of dielectric image line array antennas.**

I. INTRODUCTION

IN RECENT years, several components for use in dielectric waveguide-integrated millimeterwave circuits have been developed. Semiconductor devices and their associated tuning and matching arrangements and especially mode launchers have been noted for their inherent radiation losses. To reduce the radiation effects in semiconductor circuits, metallic shielding is used (metal waveguide housing) and metal waveguide horn transitions are used as mode launchers [1]. A different approach to circumvent radiation losses uses periodic structures in the radiation-free stopband mode as tuning and matching devices [2], [3], or Yagi–Uda arrays as mode launchers [4].

In this paper slots in the ground plane of the dielectric image line are investigated for applications as mode launchers or discontinuity circuit elements. The main attraction of the proposed structure is that dielectric layer above the slots due to total reflection from the dielectric–air interface can act as a partial shielding, thus reducing radiation losses.

Manuscript received June 5, 1980; revised August 28, 1980. This work was supported by the German Research Society under Contract Wo 137/6.

The author is with University Duisburg, Fachgebiet Allgemeine und Theoretische Elektrotechnik, FB 9, Bismarckstrasse 81, 4100 Duisburg, Federal Republic of Germany.

0018-9480/81/0100-0010$00.75 ©1981 IEEE

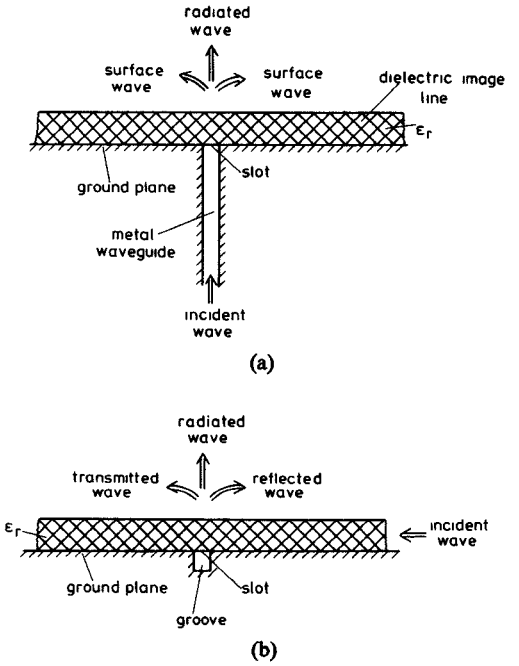

Fig. 1. (a) The slot as a mode launcher. (b) The groove as a line discontinuity.

II. The Slot Structures

The proposed slot structures are sketched in Fig. 1. In Fig. 1(a) a mode launcher is shown with a wave incident from a metal waveguide below the dielectric image line. The wave is coupled into the dielectric image line through a slot in the ground plane of the dielectric image line. The incident power is partly coupled into the surface waves on the dielectric waveguide and partly is radiated into the space above the dielectric image line. In Fig. 1(b) a groove in the ground plane of the dielectric image line acts as a line discontinuity. The incident wave on the dielectric image line partly is reflected by the slot discontinuity, partly is radiated into the space above the dielectric waveguide and partly is transmitted across the slot.

The aim of this paper is to determine a suitable equivalent circuit for both cases. As readily can be seen, the structures in Fig. 1 basically are T-junctions of a dielectric image line and a metal waveguide. In Fig. 1(a) all of the joining waveguides are considered infinitely long, whereas in Fig. 1(b) the metal waveguide arm of the junction is short-circuited.

Since a rigorous solution of this complicated three-dimensional field problem poses severe difficulties it was decided to solve only a planar field problem, where the structures in Fig. 1 are independent of the direction perpendicular to the plane of paper. Of course the results will only be of approximate nature when applied to the realistic three-dimensional case of finitely wide dielectric image lines with finitely wide slots in the ground plane.

Furthermore, for the solution of the reduced field problem with respect to simplicity of formulation and ease of numerical evaluation a resonator approach was employed. In Fig. 2(a) the investigated resonator structure is shown. Here the dielectric image line is terminated by conducting

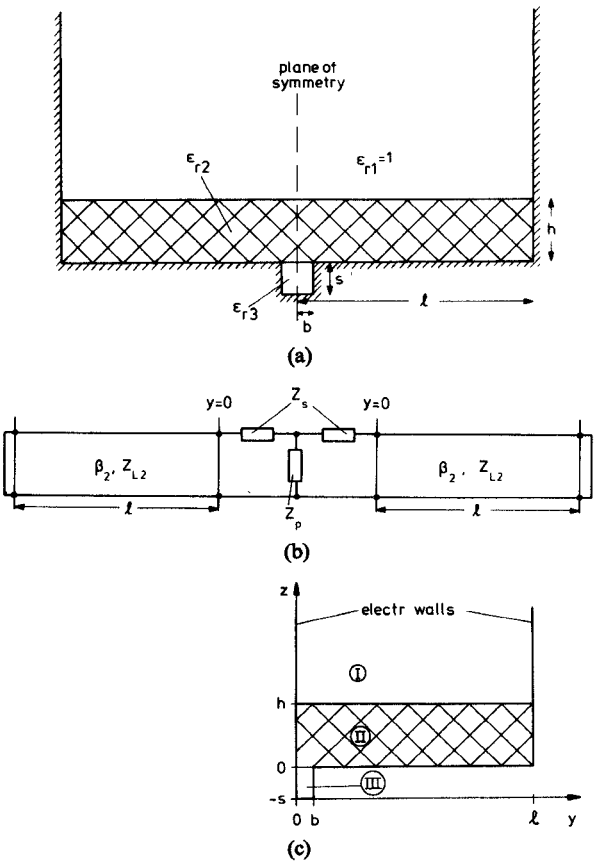

Fig. 2. (a) The resonator structure with reflecting walls and a groove beneath the dielectric image line. (b) The corresponding equivalent circuit. (c) The model resonator used for the calculation of the series slot impedance.

walls perpendicular to the ground plane and the metal waveguide arm of the T-junction is short-circuited after a length s. The fields of this structure due to its symmetry and its side walls are identical to those in an infinitely long dielectric image line with even-mode excited equidistantly spaced slots in the ground plane. That means, the model resonator will yield the characteristics of coupled slots in long arrays, as used, e.g., in leaky wave antennas. For the determination of the circuit elements of an isolated single slot the distance l of the reflector walls must be chosen very large in order to reduce its effect on the slot radiating fields [5].

A suitable equivalent circuit representation of the resonator structure is shown in Fig. 2(b). Here the slot discontinuity is represented by a T-section. Since only narrow slots shall be investigated the parallel impedance Z_p may be neglected and only the series impedances Z_s have to be considered. This is done by choosing the plane of symmetry to be an electric wall as shown in Fig. 2(c).

In the Appendix, for the three regions of the model resonator of Fig. 2(c) complete sets of fields solutions are derived and by satisfying the boundary conditions at $z=h$ and $z=0$ the eigenvalue equation is derived. The solution to the eigenvalue equation is the resonance frequency f_0 of the resonator structure. In the undisturbed resonator (vanishing groove depth $s=0$) the resonance frequency $f_0=f_{0u}$ is purely real, while for finite depth of the groove

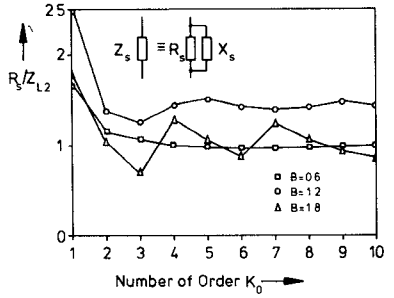

Fig. 3. The calculated normalized slot radiation resistance versus the number of order of the employed resonators with the normalized frequency $B=4h\sqrt{\epsilon_{r2}-1}\,/\lambda_0$ as the parameter.

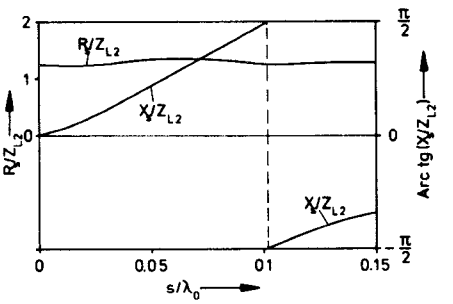

Fig. 4. The calculated normalized slot radiation resistance and the normalized slot reactance versus the normalized groove depth.

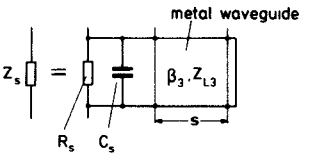

Fig. 5. The derived approximate equivalent circuit for the slot series impedance.

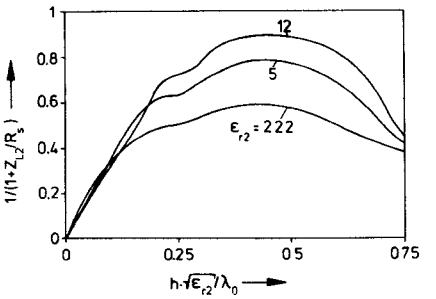

Fig. 6. The calculated normalized slot radiation resistance versus the normalized height of the dielectric image line with the relative permittivity of the dielectric image line as the parameter.

($s>0$) the resonator leaks power into the space above the dielectric waveguide and the resonance frequency turns complex: $f_0 = f_0' + jf_0''$. The imaginary part f_0'' accounts for the radiation losses due to the slot fields.

As can be shown, a comparison of the calculated resonance frequencies of the undisturbed resonator and the disturbed resonator yields the slot series impedance Z_s as

$$Z_s = -jZ_{L2}\tan\left(K_0\pi\frac{f_0'+jf_0''}{f_{0u}}\right) \qquad (1)$$

where K_0 (number of order) is the number of half-wavelengths inside the undisturbed resonator, $l = K_0\cdot\lambda_2/2\cdot Z_{L2}$ is the characteristic impedance of the dielectric image line. The convergence properties of the method have been investigated and it has been found out that for a satisfactory relative accuracy of the calculated series impedance Z_s the number of modes considered in the field expansions of regions I and II need to be $2K_0$ up to $6K_0$ while in region III in all cases examined three modes are satisfactory ($N=3$). In the following for reasons of better physical understanding a parallel configuration of the imaginary part X_s and the real part R_s of the slot impedance Z_s is assumed as indicated in the inset of Fig. 3. It was found that the number of order K_0, i.e., the distance of the slots from the reflecting walls has no appreciable effect on X_s, while it has a major effect on the calculated resistance R_s, as can be seen from Fig. 3.

The reason for this is that the imaginary part of Z_s represents the energy which is stored inside and near the slot, while the real part of Z_s can be interpreted as the radiation resistance of the slot since it represents the power radiated from the slot. It is clear that the mutual radiation resistance of the slot and his image (represented by the reflector walls) will lead the variations in the slot resistance as long as the images are near the slot. So, for the calculation of the radiation resistance R_s of isolated single slots long resonators have to be considered with $K_0 \geqslant 10$, or the asymptotical value of R_s for a series of shorter resonators has to be evaluated. Since the size of the system matrix increases proportional to K_0^2 the numerical effort is very high when isolated slots are investigated. In the computations a maximum matrix size of 50×50 was maintained with low accuracies of several percent for the radiation resistance in some cases.

In Fig. 4 the calculated slot radiation resistance R_s as well as the slot reactance X_s are plotted versus the depth s of the groove. Analyses of this relationship have led to the equivalent circuit for the slot as shown in Fig. 5. The slot radiation resistance is assumed independent from the groove depth s while the slot reactance is assumed to be the sum of the reactance due to a short-circuited metal waveguide (groove) and the fringing capacitance in the plane of the slot. Thus the slot discontinuity simply is described by an ideal T-junction with the real resistance R_s and the capacitance C_s connected across the metal waveguide arm of the junction.

Though this result may not be surprising from analogy considerations with respect to metal waveguide T-junctions, the magnitude of the radiation resistance R_s is most interesting to investigate. Due to the dielectric–air interface at $z=h$ part of the power radiated from the slot is reflected back into the dielectric guide. Thus the radiation resistance has to be expected to be a function of both the height h of the dielectric and the relative permittivity ϵ_{r2}. In Fig. 6 the calculated normalized form of the radiation resistance R_s/Z_{L2} is plotted versus the two mentioned parameters.

It can be seen that R_s/Z_{L2} increases with increasing dielectric constant, i.e., the radiation losses decrease. This accounts for the increase of the reflection coefficient of the dielectric–air interface with increasing dielectric constant. Furthermore Fig. 6 shows that the radiation losses are a minimum for a dielectric guide with a normalized height $h\cdot\sqrt{\epsilon_{r2}}/\lambda_0\approx 0.4$. This accounts for the interference effects of waves radiated directly from the slot and indirect waves (from reflection at the dielectric–air interface and at the ground plane).

III. Launching Efficiency

A. Theoretical Evaluation

The launching efficiency of the mode launcher sketched in Fig. 1(a) can now be discussed employing the results of Section II. The equivalent circuit representation for the mode launcher is given in Fig. 7(a) for the bilateral launching configuration, where the wave incident from the wave source on the metal waveguide side of the T-junction launches surface waves in both directions of the dielectric image guide. In Fig. 7(b) the representation is given for the unilateral launching configuration where one side of the dielectric image line is short-circuited in a half wavelength distance from the slot launcher.

It may be assumed that for narrow slots ($b \ll \lambda$) the field distribution of the slot discontinuity is very similar to that of the slot in the resonator configuration treated in Section II. Thus in Fig. 7 the slot discontinuity is represented by the slot impedance Z_s.

The launching efficiency η is the ratio of the power P_{sw} launched on the dielectric waveguide and the total power P_{tot} delivered to the slot. Using Fig. 7 the bidirectional launching efficiency η_{bi} can be derived as

$$\eta_{bi} = \frac{2P_{sw}}{P_{tot}} = \frac{1}{1+1/(R_s/Z_{L2})} \tag{2}$$

while the unidirectional launching efficiency η_{uni} yields

$$\eta_{uni} = \frac{P_{sw}}{P_{tot}} = \frac{1}{1+1/(2R_s/Z_{L2})}. \tag{3}$$

The derived expression for the bilateral launching efficiency η_{bi} can be seen to be identical to the normalization for the slot radiation resistance used in Fig. 6. Thus Fig. 6 is a plot of the bilateral launching efficiency η_{bi}. As can be seen from (2) and (3) the unilateral launching efficiency η_{uni} is higher than the bidirectional launching efficiency η_{bi}. This important result has been found for other mode launching configurations too [6].

In Table I the optimum achievable values ($h\sqrt{\epsilon_{r2}}/\lambda_0\approx 0.4$) of both efficiencies are listed for three different values of the dielectric constant ϵ_{r2}. It can be seen from the table that the unidirectional launching efficiency is about the square root value of the bidirectional launching efficiency. The absolute values of the unidirectional launching efficiency are equal to or better than the efficiencies measured for conventional metal waveguide horn launchers (usually in the order of -0.5 dB to -1.5 dB, depending on the horn length and flare) or other types of mode launchers [6].

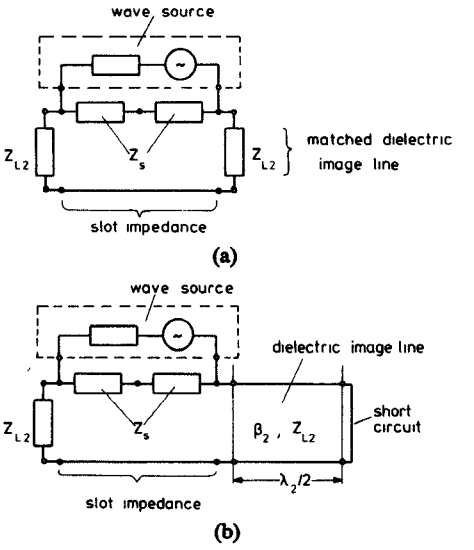

Fig. 7. (a) The equivalent circuit representation for the bidirectional slot mode launcher. (b) The unidirectional slot mode launcher.

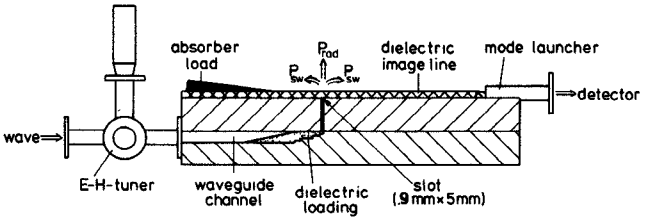

Fig. 8. The measurement setup used for the experimental determination of the launching efficiency.

TABLE I
The Calculated Optimum Bidirectional and Unidirectional Slot Launching Efficiencies for Various Relative Permittivities of the Dielectric Image Line

ϵ_{r2}	η_{bi}	η_{uni}
12	-0.48 dB	-0.25 dB
5	-1.05 dB	-0.56 dB
2.22	-2.26 dB	-1.28 dB

B. Experimental Verification

For the experimental verification of the theoretically calculated launching efficiencies a measurement setup sketched in Fig. 8 was used. Here, the T-junction consists of a dielectric image line terminated by an absorber load on one side and a horn transition to a metal waveguide detector on the other side. The slot in the ground plane is excited via a waveguide channel milled into the ground plane block. To achieve a match at the slot plane and to tune out reflections from the stepped impedance transformer of the waveguide channel an *EH*-tuner was employed at the input flange. Furthermore the transmission losses of the channel and of the horn transition were measured separately. The ratio of the excited surface wave power $2P_{sw}$ and the total incident power $P_{tot}=2P_{sw}+P_{rad}$ was measured for several low-permittivity dielectric image

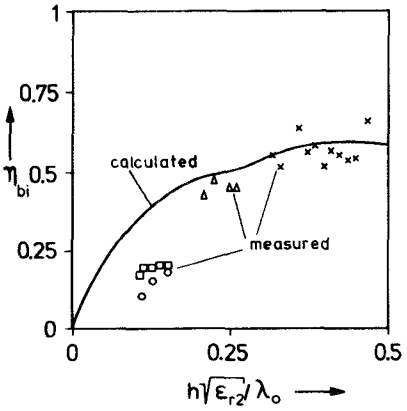

Fig. 9. The measured and calculated bidirectional launching efficiencies of a slot mode launcher versus the normalized height of the dielectric image lines. Several dielectric image lines of low permittivity ($\epsilon_{r2} \approx 2.3$) and of variable height h were employed in the experiments. The half-width/height-ratio (w/h) of the lines was ×: $w/h=1$, △: $w/h=3$, ○: $w/h \approx 5$, □: $w/h \approx 10$.

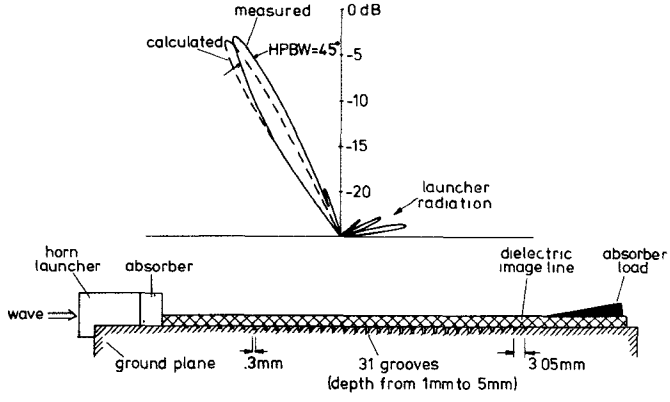

Fig. 10. Sketch of the experimental 60-GHz dielectric image line slot antenna with the measured and the predicted radiation patterns in the E-plane of the antenna.

guides of normalized height $0 < h\sqrt{\epsilon_{r2}}/\lambda_0 < 0.5$.

The bidirectional launching efficiency η_{bi} was calculated using $\eta_{bi} = 2P_{sw}/P_{tot}$ and was plotted together with the theoretical predictions in Fig. 9. As can be seen, agreement is good, especially for those guides having the optimum normalized height near $h \cdot \sqrt{\epsilon_{r2}}/\lambda_0 = 0.4$.

IV. Circuit Elements

Besides employing the described slot structure as a mode launcher several other applications in dielectric image line circuits can be realized. The slot structure could house, e.g., semiconductor devices or a movable short circuit for tuning and matching purposes. Perhaps the most appropriate application would be in periodic structures (stopband filter) or in dielectric image line slot array (or leaky-wave) antennas. In periodic structure stopband filters a large number of grooves in the ground plane are arranged equidistantly along the dielectric image line (distance about one half guide wavelength). The bandwidth of the filter can be controlled through the slot impedance, i.e., by choosing the depth and width of the grooves. In slot array antennas a number of grooves are arranged below the dielectric guide with the distances of the grooves greater than one half guide wavelength to produce a beam in the upper half space. In order to realize a prescribed aperture distribution along the length of the antenna the groove depth s can be varied so that the slot radiation resistances R_s of the individual slots are shunted by reactances of variable magnitude.

In a first experimental slot antenna for 60 GHz a smooth variation of the groove depth was chosen as indicated in Fig. 10. The distances of the 31 slots were about 2/3 of a guide wavelength without variations to compensate for the phase variations due to the reactive parts in the slot impedances. 30-mm long transverse grooves were milled into a brass ground plane using a circular saw blade of 0.3-mm width. The dielectric guide of 3-mm by 0.8-mm cross section was cut from a RT/Duroid substrate and fixed to the ground plane using a thin film adhesive. The dielectric image line was excited through a horn mode launcher with a piece of absorbing foam in the mouth of the horn in order to attenuate the direct radiation from the launcher.

The measured and calculated H-plane radiation pattern of the slot antenna is also given in Fig. 10. The agreement of the experimental and the theoretical pattern is satisfactory considering the approximate nature of the used basic slot equivalent circuit and the fact that the phase variation due to the variable slot reactances is not compensated in the design of the antenna.

It was found that the length of the antenna was overdesigned since about 90 percent of the incident power is radiated by the first 23 slots. Thus a much shorter antenna could be realized with the same properties as the present one. Also, there are some major sidelobes in the measured radiation pattern at near endfire angles which are produced by direct radiation from the horn launcher. These lobes can be reduced by using a larger foam absorber to load the horn mouth.

V. Conclusion

In this paper slots in the ground plane of the dielectric image line were investigated as mode launchers or discontinuity circuit elements. Surface waves can be excited through a metal waveguide terminating in a slot in the ground plane of a dielectric image line. The slot equivalent circuit representation is approximately calculated using a planar resonator model. It is found that the slot discontinuity can be represented by a T-junction of the dielectric image line and a metal waveguide. The radiation losses are represented by a resistance bridging the junction. The launching efficiency is found to increase with the dielectric constant of the dielectric image line, exhibiting a maximum value for guides of slightly smaller height than half a wavelength in the dielectric medium. The measured and calculated launching efficiencies of low permittivity dielectric image lines are found in good agreement.

Grooves can be employed as discontinuity circuit elements. As an example a dielectric image line slot antenna

using transverse grooves in the ground plane beneath the dielectric guide is presented. The measured radiation pattern of the experimental antenna exhibits satisfactory agreement with the predicted pattern. Critical points in the antenna design are the need for a compensation for the slot reactances and the dimensions of the absorber used to reduce the endfire radiation from the mode launcher. Several other applications of the proposed slot structures in dielectric image line are possible, such as filters or semiconductor circuits.

Appendix

The Resonator Eigenvalue Equation

The fields of the resonator of Fig. 2(c) are derived from E^y-potentials to describe the fundamental TM-mode characteristics of the slot discontinuity. The series expansion of the potential functions in the three field regions are

$$\Pi^{\mathrm{I}} = \sum_{k=0}^{\infty} F_k \cos\left(\frac{k\pi}{l}y\right) e^{-\gamma_k z}$$

$$\Pi^{\mathrm{II}} = \sum_{k=0}^{\infty} \cos\left(\frac{k\pi}{l}y\right)\left[B_k \cos(\beta_{zk} z) + B'_k \sin(\beta_{zk} z)\right]$$

$$\Pi^{\mathrm{III}} = \sum_{n=0}^{\infty} H_n \cos\left(\frac{n\pi}{b}y\right)\sin((z+s)\beta_{zn}) \qquad \text{(A.1)}$$

where

$$k_0^2 = \left(\frac{k\pi}{l}\right)^2 - \gamma_k^2$$

$$k_0^2\epsilon_{r2} = \left(\frac{k\pi}{l}\right)^2 - \beta_{zk}^2$$

$$k_0^2\epsilon_{r3} = \left(\frac{n\pi}{b}\right)^2 + \beta_{zn}^2 \qquad \text{(A.2)}$$

and $k_0 = 2\pi/\lambda_0 = 2\pi/c_0 \cdot f =$ wavenumber of free space. The E_y-field strengths and the transversal H_x- and E_z-field strengths can be derived from the potentials using well-known methods, e.g., [7].

The amplitude coefficients F_k, B_k, B'_k, and H_n have to be chosen in such a way that the continuity conditions for the tangential fields are satisfied. For the plane $z=h$ this condition leads to the well-known eigenvalue equation for the TM-modes on the dielectric slab guide

$$S(k)\cdot B_k + S'(k)\cdot B'_k = 0 \qquad \text{(A.3)}$$

with

$$S(k) = \frac{\beta_{zk}}{\gamma_k}\cos(\beta_{zk} h) + \epsilon_{r2}\sin(\beta_{zk} h)$$

$$S'(k) = \frac{\beta_{zk}}{\gamma_k}\sin(\beta_{zk} h) - \epsilon_{r2}\cos(\beta_{zk} h)$$

for all $k = 0, 1, 2, \cdots$.

A zero of the term $S(k)$ is the resonance condition for an even TM-mode (i.e., a mode with $E_y \neq 0$ in plane $z=0$), whereas a zero of $S'(k)$ is the resonance condition for an odd TM-mode (i.e., a mode with $E_y = 0$ in plane $z=0$). The coupling of even and odd modes and the coupling of the fundamental modes with higher order modes is caused by the slot in the conducting ground plane as is shown in the following.

In the plane of the slot $z=0$ the continuity condition for the electric field strength is

$$E_y^{\mathrm{II}} = \begin{cases} E_y^{\mathrm{III}}, & y \leqslant b \\ 0, & y > b \end{cases}. \qquad \text{(A.4)}$$

This condition is satisfied employing the least squares method, e.g., [7] and leads to

$$B_k = \frac{1}{\beta_{zk} l}\sum_{n=0}^{\infty} H_n \beta_{zn}^2 \sin(\beta_{zn} s)\delta_k \cdot \int_0^b \cos\left(\frac{n\pi}{b}y\right)\cos\left(\frac{k\pi}{l}y\right) dy \qquad \text{(A.5)}$$

with

$$\delta_k = \begin{cases} 1, & \text{for } k=0 \\ 2, & \text{for } k\neq 0 \text{ and } k = 0, 1, 2, \cdots. \end{cases}$$

For the tangential magnetic field strength the continuity condition is

$$H_x^{\mathrm{II}} = H_x^{\mathrm{III}}, \qquad y \leqslant b \qquad \text{(A.6)}$$

which again is satisfied using a least squares condition and for all $n = 0, 1, 2, \cdots$ leads to

$$H_n = \frac{\epsilon_{r2}}{\epsilon_{r3}\beta_{zn}\cos(\beta_{zn} s) b} \cdot \sum_{k=0}^{\infty} B'_k \beta_{zk}\delta_n \int_0^b \cos\left(\frac{n\pi}{b}y\right)\cos\left(\frac{k\pi}{l}y\right) dy \qquad \text{(A.7)}$$

with

$$\delta_n = \begin{cases} 1, & \text{for } n=0 \\ 2, & \text{for } n\neq 0 \end{cases}.$$

The construction of the eigenvalue equation for the complete resonator structure is best performed using matrix formulation of the derived continuity conditions. Equation (A.3) can be written as

$$\vec{\vec{S}}\cdot\vec{B} + \vec{\vec{S}}'\cdot\vec{B}' = 0 \qquad \text{(A.8)}$$

where $\vec{\vec{S}}$ and $\vec{\vec{S}}'$ are diagonal matrices with $S(k)$ and $S'(k)$ as the diagonal elements and $\vec{B}$ and $\vec{B}'$ are the amplitude vectors. Analoguosly, (A.5) can be written as

$$\vec{B} = \vec{\vec{R}}\cdot\vec{H} \qquad \text{(A.9)}$$

and (A.7) converts into

$$\vec{H} = \vec{\vec{Q}}\cdot\vec{B}'. \qquad \text{(A.10)}$$

The mode coupling in the disturbed resonator can now be described by inserting (A.10) into (A.9)

$$\vec{B} = \vec{\vec{R}}\cdot\vec{\vec{Q}}\cdot\vec{B}' = \vec{\vec{P}}\cdot\vec{B}' \qquad \text{(A.11)}$$

where $\vec{\vec{P}} = \vec{\vec{R}}\cdot\vec{\vec{Q}}$, and inserting (A.11) into (A.8)

$$(\vec{\vec{S}}\cdot\vec{\vec{P}} + \vec{\vec{S}}')\cdot\vec{B}' = 0. \qquad \text{(A.12)}$$

Equation (A.12) is the eigenequation of the disturbed resonator. $\vec{\vec{S}}'$ represents the uncoupled eigenmodes of the undisturbed resonator (if $s=0$), while the product $\vec{\vec{S}}\cdot\vec{\vec{P}}$

describes the effect of the slot discontinuity, i.e., the coupling of the eigenmodes of the undisturbed structure. The eigenvalues, i.e., the resonance frequencies of the resonator are found if the eigenvalue equation

$$\det(\overleftrightarrow{S}\cdot\overleftrightarrow{P}+\overleftrightarrow{S'})=0 \qquad \text{(A.13)}$$

is satisfied, that means if the zeros of the system determinant are found.

References

[1] R. M. Knox, "Dielectric waveguide microwave integrated circuits—an overview," *IEEE Trans. Microwave Theory Tech.*, vol. MTT-24, Nov. 1976, pp. 806–814.

[2] T. Itoh and F.-J. Hsu, "Distributed bragg reflector gunn oscillators for dielectric millimeter-wave integrated circuits," *IEEE Trans. Microwave Theory Tech.*, vol. MTT-27, May 1979, pp. 514–518.

[3] K. Solbach, "Grating-tuner in dielectric image line for integrated millimeterwave circuits," *Dig. 9th European Microwave Conf.*, (Brighton, England), pp. 458–462, Sept. 1979.

[4] W. K. McRitchie and J. C. Beal, "Yagi-Uda array as a surface-wave launcher for dielectric image lines," *IEEE Trans. Microwave Theory Tech.*, vol. MTT-20, Aug. 1972, pp. 493–496.

[5] J. Galejs, "Driving point impedance of linear antennas in the presence of a stratified dielectric," *IEEE Trans. Antennas Propagat.*, vol. AP-13, Sept. 1965, pp. 725–736.

[6] R. H. Duhamel and J. W. Duncan, "Launching efficiency of wires and slots for dielectric rod waveguide," *IRE Trans. Microwave Theory Tech.*, vol. MTT-6, Mar. 1958, pp. 277–284.

[7] R. F. Harrington, *Time-harmonic electromagnetic fields*. New York: McGraw-Hill, 1961.

Propagation Properties of a Planar Dielectric Waveguide with Periodic Metallic Strips

KAZUHIKO OGUSU, MEMBER, IEEE

***Abstract*—A dielectric waveguide with periodic metallic strips suitable for millimeter-wave and submillimeter-wave integrated circuits is analyzed by a rigorous formulation. The accuracy of the solution of our analysis can be systematically improved by increasing the size of the matrix associated with the eigenvalue equation. Stopband properties are numerically presented as a function of the spacing and width of metallic strips and dielectric profile. It is found that there is a difference in the stopband properties of TM and TE modes. Experimental results for the band reject filter are also presented to verify the validity of our analysis.**

I. Introduction

DIELECTRIC periodic structures have been applied to many devices in integrated optics, such as filters [1], [2], input and output beam couplers [3], [4], and distributed feedback lasers [5]. At millimeter and submillimeter wavelengths too, they can be applied to devices similar to those in integrated optics. Although a few investigations have been reported [6], periodic structures have not yet been widely used in millimeter-wave and submillimeter-wave integrated circuits.

The purpose of the present paper is to determine the propagation properties of a planar dielectric waveguide with periodic metallic strips as shown in Fig. 1. This periodic structure can be easily and accurately fabricated by existing printed-circuit techniques for microstrip microwave integrated circuits and is suitable for millimeter-wave and submillimeter-wave integrated circuits. The propagation properties are characterized by the film thickness, width and spacing of metallic strips, dielectric profile, and operating frequency. We restrict the discussion to the stopband phenomenon applicable to band reject filters, since the scattering properties of similar periodic structures with metallic strips are discussed in several articles and texts [7]–[9]. The theoretical analysis is essentially the same as the spectral domain approach [10], [11], which is a powerful tool for the analysis of striplines.

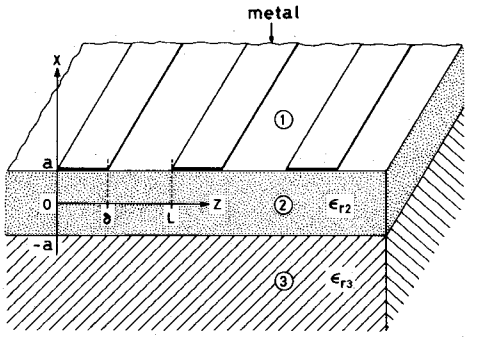

Fig. 1. Geometry of the dielectric waveguide with periodic metallic strips. Regions 1, 2, and 3 correspond to a cover (air), guiding film, and substrate, respectively.

The width and center frequency of the stopband and attenuation constant at the center frequency are numerically presented as a function of the width and spacing of the metallic strips and dielectric profile. It is found that there is a difference in the stopband properties of TM and

Manuscript received December 6, 1979; revised August 27, 1980.

The author is with the Faculty of Engineering, Shizuoka University, Hamamatsu, 432 Japan.

0018-9480/81/0100-0016$00.75 ©1981 IEEE